Nanoscale

Accepted Manuscript

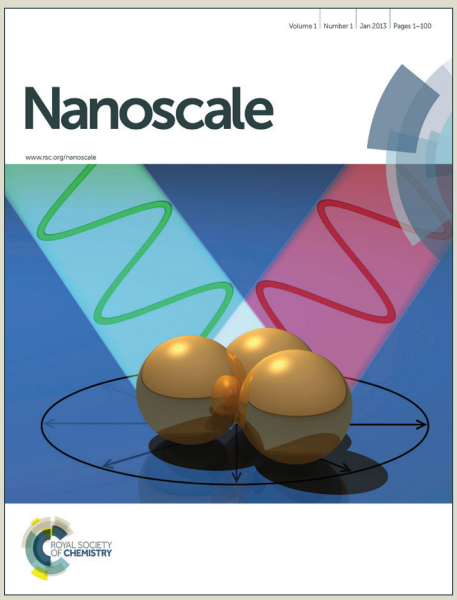

ROYAL SOCIETY OF CHEMISTRY

www.rsc.org/nanoscale

www.rsc.org/xxxxxx

ARTICLE TYPE

Induction Phenomenon and Catalytic Deactivation of Thiolate-stabilized Raspberry-like Polymer Composites Coated with Gold Nanoparticles

Maolin Li,[a] Guofang Chen,*[a] and Shiper Bhuyain [a]

Alkylthiolate ligands act as dual roles in metal nanoparticles-coated polymer composite catalysts: stabilizer and deactivator. Herein, individual raspberry-like polymer composite spheres coated with gold nanoparticles were separated from each other in the presence of 6-mercaptohexanoic acid or 3-mercaptopropionic acid ligands. Effects of thiolate ligands on the induction time and the catalytic activity of such non-aggregated polymer composites were investigated experimentally and theoretically in the 4-nitrophenol/$NaBH_4$ model reaction from the following aspects: ligand surface coverage, chain order and the chain length. With the increase in alkylthiolate surface coverage and chain order on composite particles, the induction time increases first and then decreases, which can be explained based on spontaneous dynamic surface restructuring and electron injection from borohydride ions to gold nanoparticle surface. The catalytic activity is compromised with the existence of thiolate ligands, but is enhanced with increasing alkylthiolate ligand coverage, which can be ascribed to sulfur-induced electronic charge depletion of the gold nanoparticles. The increment of CH_2 in alkylthiolate chains results in the increase of induction time and the decrease of the catalytic activity, which can be attributed to steric hindrance effect. The reactant addition sequence was also found to affect the induction time and the catalytic activity, which can be partially credited to $NaBH_4$ reductant-induced desorption of thiolate ligands.

1. Introduction

Induction phenomenon is common in heterogeneous catalysis reaction: there is always a time lag before reaction occurs when all the reactants are mixed together, which is related to the so-called "induction time" required for the catalyst activation.[1-14] The factors affecting the induction time can be diverse: diffusion-controlled adsorption of reactants onto the surface of metal catalyst,[8, 9] dissolved oxygen competition with the reactants,[10, 15, 16] slow surface restructuring of metal catalyst,[11, 12] and/or electron injection from reducing agent to the metal catalyst.[17] Recently colloidal metal nanoparticles exhibit exceptional properties in heterogeneous catalysis reaction such as their ability to accelerate reactions that do not occur under normal conditions, excellent selectivity, and recyclability.[18, 19] However, because of their high surface energies, free-standing colloidal metal nanoparticles or nanoparticles on the supporting material tend to aggregate and then drop, or change shape in liquid-phase catalytic reactions so that their activity and selectivity will gradually disappear after several cycles of catalysis.[20, 21] Thiolate derivatives have been used as the ligands of choice to stabilize metal nanoparticles and hinder aggregation due to strong sulfur-metal covalent bonding and the intermolecular interactions.[22] The alkylthiolate surface ligand consists of three parts: the sulfur headgroup for forming a strong covalent bond with the metal nanoparticles, the hydrocarbon chain of variable length to stabilize the monolayer through van der Waals interactions, and the terminal group with different functionalities. However, earlier studies found that the presence of a densely packed capping layer on the metal nanoparticles surface may compromise the catalytic activity as the surface active sites become inaccessible.[23-26] Catalyst deactivation can be caused by a reduction in the number of active sites, a decrease of the quality of the active sites and/or a degradation in accessibility of the active sites. Although the correlation between catalytic activity and surface ligands of monolayer protected free-standing gold nanoparticles has been investigated,[25] the study of the effect of alkylthiolate ligands on the induction time and catalytic activity of supported gold nanoparticle, like polymer colloidal composites coated with gold nanoparticles, has not yet been explored in details. Many studies have claimed that the initial stage of thiol chemisorptions on Au (111) involves the formation of lying-down phases with molecules parallel to the substrate. Upon increase of surface coverage, a transition from the "lying-down" to a "standing-up" configuration takes place with the formation of domains of the dense and stable thiol lattices.[27] Therefore, some particularly important questions need to be addressed: how will the alkylthiolate graft density and chain order affect the induction time and the catalytic activity of the thiolate-stabilized supported gold nanoparticles? What is the relationship between the chain length of surface alkylthiolate ligand and catalytic properties of the supported gold nanoparticles? Does the sulfur-gold interface

Chemistry Department, St John's University, Queens, New York, 11439, USA. E-mail: gfchen08@yahoo.com; Fax: +1-718-990-1876; Tel: +1-718-990-8092

involve the induction phenomenon and catalytic deactivation?

Recently in our research group, a new type of gold nanoparticle-coated composite sphere, PGMA@PAH@AuNPs, based on chemically reactive poly(glycidyl methacrylate) (PGMA) colloids modified by poly(allylamine hydrochloride) (PAH) at sub-micrometer scale was successfully prepared in a raspberry-like fashion by an easy and facile controlled assembly method.[28] To prevent the as-prepared polymer colloidal composites from aggregation/dropping, alkylthiolates were used to modify the surface of the composite particles. One popular catalytic model reaction 4-nitrophenol (4-NP)/$NaBH_4$ in the presence of raspberry-like PGMA@PAH@AuNPs composites stabilized by water-soluble alkylthiolate ligands was employed to explore the effects of the graft density, chain order and chain length of surface alkylthiolate ligands, and the sulfur-metal interface on the induction time and the catalytic activity of metal nanoparticle-based system.

2. Experimental Section

2.1 Materials

Glycidyl methacrylate (≥97.0 %, Sigma-Aldrich, St. Louis, MO, USA) (GMA) was purified prior to use with a hydroquinone and monomethyl ether hydroquinone inhibitor remover (Sigma-Aldrich, St. Louis, MO, USA) and stored at a temperature of 4 °C. Potassium persulfate (99%) (KPS), poly(allylamine hydrochloride) (PAH) (M_W 15,000), 6-mercaptohexanoic acid (MHA), 3-mercaptopropionic acid (MPA) and tetrachloroaurate trihyrate ($HAuCl_4{\cdot}3H_2O$), 4-nitrophenol (4-NP), sodium borohydride as well as trisodium citrate were purchased from Sigma-Aldrich. The Nanopure water throughout use in this study was deionized by Barnstead 18.2 MΩ cm ultrapure water system (Thermo Scientific, Waltham, MA, USA). Prior to use, all glassware were cleaned by immersing in *aqua regia* solution for 30 min and rinsed with Nanopure water.

2.2 Synthesis of raspberry-like PGMA@PAH@AuNPs sub-microspheres

First of all, the PGMA colloids (448 ± 9 nm) were synthesized by surfactant-free emulsion polymerization method in our previous publication.[29] Briefly, 15 mL of inhibitor removed monomer GMA was added into 150 mL of Nanopure water. The mixture was purged with N_2 while stirring at 1,200 rpm for 30 min at room temperature. Heated up to 90 °C, the reaction mixture was followed by adding 10 mL of KPS (5 % w/v) dropwise. The flow of nitrogen was reduced to minimize the stripping of monomer and was stopped after 15 min. After 2 h of polymerization maintained at 1,200 rpm and 90 °C, the reaction was stopped by oxygen purging for 30 min. After cooling to room temperature and dialyzing in a Cellulose Ester Dialysis membrane (MWCO 3,500-5,000, Spectrum Laboratory, Inc, Rancho Dominguez, CA) for 24 h with 3 times of water change, the solution was centrifuged to remove the supernatant and redispersed in water. Furthermore, the 12 ± 3 nm citrate-stabilized AuNPs were prepared by reduction of $HAuCl_4{\cdot}3H_2O$ using trisodium citrate that acts as both a reducing and a capping agent according to the Turkevich method.[30] Finally, PGMA@PAH sub-microspheres were prepared in the way similar to our previous work.[28] Specifically, 10 mL of purified PGMA spheres were mixed with 1 mL PAH solutions with different concentrations. The PGMA@PAH dispersion solutions were obtained by electrostatic attraction between negatively charged PGMA spheres and weak positively charged hydrophobic PAH polyeletrolyte solutions. Two batches of 0.6 mL of PGMA@PAH dispersion solution 0.5 % (w/v) at pH = 7 were chosen to suspend in 60 mL of pristine AuNPs solution, respectively, for saturated adsorption of AuNPs through electrostatic attraction between AuNPs and PGMA@PAH with opposite charges to form PGMA@PAH@AuNPs composites in a raspberry-like fashion. All samples were mixed by gentle shaking at around 1,000 rpm for 30 min on a SH 2,000 Fine mixer shaker (Daigger, Vernon Hills, IL, USA). The PGMA@PAH@AuNPs composites were collected after centrifugation and re-dispersed in Nanopure water. The as-preformed PGMA@PAH@AuNPs composite microspheres were then divided into 6 equal portions for further use.

2.3 Preparation of thiolate-stabilized PGMA@PAH@AuNPs sub-microspheres

0.5% (w/v) PAH-modified-PGMA@AuNPs (12 ± 3 nm AuNPs) at pH = 7 composite particles stabilized by MHA or MPA were prepared by centrifugation of 10 mL pre-synthesized 0.5 % (w/v) PAH-modified PGMA@AuNPs composite particles at 2,000 rpm, and redispersed in 10 mL of MHA or MPA aqueous solutions, respectively at various concentrations (0.454 mM, 0.113 mM, 0.0567 mM, 0.0284 mM and 0.00709 mM). The concentration of 0.454 mM alkylthiolate solution was obtained based on 1 : 1 mole ratio of thiolate to gold atom on composite particles. All sample solutions were mixed by gentle shaking at around 1,000 rpm for 30 min on a SH 2,000 Fine mixer shaker and settled for 1 h. The mixture solution was centrifuged and washed with Nanopure water twice to remove the non-adsorbed alkylthiolates and finally redispersed in 10 mL Nanopure water.

2.4 Kinetic studies of 4-NP reduction and thiolate deactivation effects on the catalytic properties

The catalytic properties and thiolate deactivation effects of the thiolate modified PGMA@PAH@AuNPs composites were examined by 4-NP/$NaBH_4$ catalytic redox model reaction. Namely, 1.25 mL of 4-nitrophenol aqueous solution (0.1 mM) and 0.5 mL of freshly prepared $NaBH_4$ aqueous solution (0.1 M) were first mixed and stirred for 1-2 min in a 3 mL quartz cuvette at 298 K. To this mixture, 0.4 mL alkylthiolate (MHA or MPA)-stabilized PGMA@PAH@AuNPs composites containing 3.32×10^{-12} mole of AuNPs was added and mixed thoroughly, and the control experiment was conducted with 0.4 mL original composites. The reduction in the optical absorption peak of 4-NP (400 nm) was determined from the UV-Vis spectra by using a UV-Vis spectrophotometer at a 2-second scan rate. To study the effect of addition sequence of reactant components on catalytic activity, the experiments were performed in three conditions: **Sequence I**: 1.25 mL of 0.1 mM 4-NP was firstly mixed with 0.4 mL of the alkylthiolate-stabilized PGMA@PAH@AuNPs composite solution, and then 0.5 mL of 0.1 M $NaBH_4$ aqueous solution was added to initiate the reaction; **Sequence II**: 1.25 mL of 0.1 mM 4-NP was mixed with 0.5 mL of 0.1 M $NaBH_4$ firstly, followed by addition of 0.4 mL of alkylthiolate-stabilized PGMA@PAH@AuNPs composite catalysts to start the reaction

and **Sequence III**: addition of 1.25 mL of 0.1 mM 4-NP solution to a mixture of 0.5 mL of 0.1 M $NaBH_4$ and 0.4 mL of alkylthiolate-stabilized PGMA@PAH@AuNPs composite solution.

2.5 Characterization

UV-Vis spectra were recorded using an Agilent 8453 UV-Visible diode array spectrophotometer (Agilent Technologies, Santa Clara, CA, USA). JEM-1400 transmission electron microscope (TEM) (JEOL, Peabody, MA, USA) at an accelerating voltage of 120 kV was used to characterize morphology of the composite particles. All samples were prepared by placing 50 µL of the sample solution onto a carbon film coated copper grids (Electron Microscope Sciences, Hatfield, PA, USA) upon drying at room temperature. The XRD pattern was recorded in a Shimadzu LabX XRD-6000 X-ray diffractometer with Cu (Kα = 1.54060) radiation (Shimadzu Scientific Instruments, Columbia, MD, USA). The thermal stability of the composite particles was investigated by thermogravimetric analysis (TGA) (TA-Q500 instrument). The deposited amount of AuNPs on the PGMA@PAH spheres and the effects of alkylthiolate ligands on the amount of AuNPs were also investigated by TGA analysis. Samples were heated from room temperature to 700 ^oC at a constant heating rate of 10 ^oC min^{-1} under air. The flow rate was kept at 60 mL min^{-1}.

3. Results and Discussion

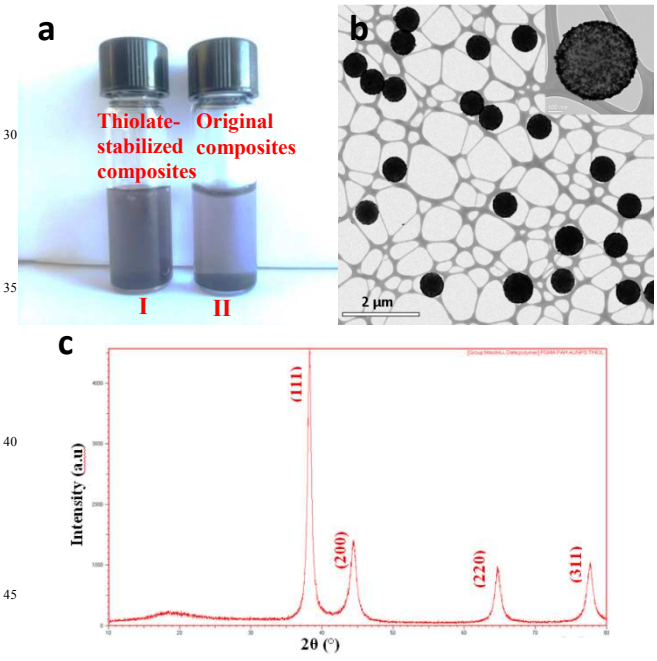

Figure 1 (a) MHA(0.454 mM)-stabilized PGMA@PAH@AuNPs composite particle solutions and original composite particle solutions settled for 30 min upon stirring. PAH concentration = 0.5% (w/v), the ratio of PGMA@PAH to AuNPs = 1 : 100 (v/v); (b) TEM images of MHA(0.454 mM)-stabilized PGMA@PAH@AuNPs composite particles, inset micrograph depicts one zoom-in composite particle image; and (c) XRD pattern of thiolate-stabilized PGMA@PAH@AuNPs sub-micrspheres.

3.1 Alkylthiolate-stabilized PGMA@PAH@AuNPs composite spheres

The previously reported raspberry-like polymer composite sub-microspheres coated with gold nanoparticles were easily aggregated to settle at the bottom of the vial with the appearance of black colored precipitates in vial II (**Figure 1a**), although gold nanoparticles were stable on the composite particles, without loss of gold nanoparticle coatings even after applying ultrasonication, cleaning or long term Nanopure water storage.[28] To enhance the dispersion of the composite particles in aqueous solution, alkylthiolate ligands were utilized to modify the surface of the particles. Vial I in **Figure 1a** shows that the thiolate-stabilized composite particles were well dispersed in water solution without formation of precipitates, which can be ascribed to the electrosteric repulsion among alkylthiolates on the composites. TEM image in **Figure 1b** depicts that gold nanoparticles exhibited a uniform distribution on individual alkylthiolate-stabilized PGMA@PAH@AuNPs composite particles which also successfully kept their originally round morphology integrity and were separate from each other.

The XRD pattern of the alkylthiolate-stabilized PGMA@PAH@AuNPs composite particles shown in **Figure 1c** confirms the formation of crystalline gold nanoparticles on PGMA@PAH sub-microspheres. Three characteristic peaks were observed for alkylthiolate-stabilized PGMA@PAH@AuNPs in the XRD pattern (**Figure 1c**) for Bragg's reflections at 2θ = 38.1, 44.2, 64.6 and 77.5° corresponding to the (111), (200), (220) and (311) lattice planes, respectively, for the face-centered cubic (fcc) gold lattice.

TGA analyses show the residues of the PGMA, PGMA@PAH, PGMA@PAH@AuNPs spheres at 695 ^oC were 0%, 0% and 18.9% respectively, which indicated the deposited AuNPs on the PGMA@PAH sub-microspheres was 18.9% since organic compounds were burned out and only AuNPs were left at such a high temperature under air. The deposited amount of AuNPs for the alkylthiolate ligands-stabilized PGMA@PAH@AuNPs was also obtained by TGA analyses: 19.3% and 21.1% for long-chain MHA and short-chain MPA at the concentration of 0.0284 mM respectively. When the concentration of alkylthiolate ligand was increased to 0.113 mM, the residues of alkylthiolate-stabilized polymer spheres were 18.7% and 18.8% for MHA and MPA ligands respectively at 695 ^oC under air. The details can be seen in Supporting Information. The obtained experimental results clearly demonstrate that the deposited amount of AuNPs on the polymer spheres is almost no change at the surface modification of alkylthiolate ligands under different chain lengths and different ligand surface coverages.

3.2 Alkylthiolate self-assembled monolayer (SAM) on gold nanoparticle

The self-assembled chain ordering of the monolayers on gold nanoparticles, which is controlled by the head-group identity, hydrocarbon chain length and terminal-group type, affects the functional properties of the SAMs greatly.[23] With the –COOH (the strongly hydrogen bonding group) as terminal functional group, even alkylthiolate SAMs with shorter chain length can still be induced to be in conformational order.[31] Moreover, the surface coverage of alkylthiolates also plays an important role in

www.rsc.org/xxxxxx

ARTICLE TYPE

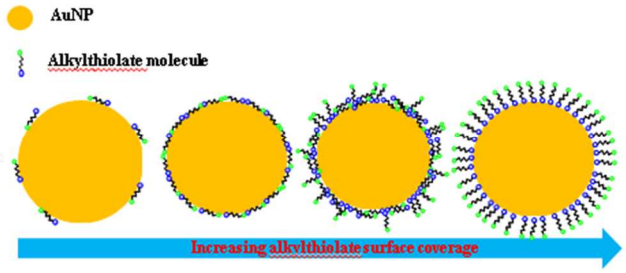

Schematic 1 The morphology change of alkylthiolate SAM on gold nanoparticles with increasing alkylthiolate surface coverage.

controlling the ordering of the SAMs.[32] **Schematic 1** manifests a graph of SAM on gold nanoparticle surface when alkylthiolate surface coverage is changed. With a relatively low thiolate surface coverage, SAM exhibits a less ordered "lying-down" configuration. When thiolate surface coverage is increased, the "standing-up" structure will be most likely to form. The "standing-up" and "lying-down" configuration can coexist on the gold nanoparticle surface. As the thiolate surface coverage is further increased, SAM starts to confine thiolate ligands into a well-organized order, and a transition from a "lying-down" to "standing-up" configuration goes to completion.[27] In addition, an increment of methylene chain in alkylthiolate can markedly enhance SAM order due to van der Waals interaction and steric effect, in addition, gauche defect in the alkyl-chain layer causes increased entropic barriers, which favors a more ordered SAM configuration.[23, 33] In this work, fundamental studies focus on the impacts of water-soluble-alkylthiolate modification to gold nanoparticles upon the induction time and the catalytic activities in the redox reaction of 4-NP/$NaBH_4$. It will epitomize the ever-lasting potential and interest in SAM-modified systems for controlling induction period and reaction rate at the site level and the diverse range of arenas in which such control is obtainable.

3.3 A typical kinetic curve for the alkylthiolate-stabilized composite spheres catalyzing heterogeneous redox reaction

The progress of reaction kinetics was monitored from the time-dependent absorption UV-Vis spectra, which showed a change in intensity of the absorption peak at 400 nm with a new peak appearing at 300 nm corresponding to 4-AP (**Figure 2a**). **Figure 2b** unveils results of a typical relationship of intensity absorption peak of 4-nitrophenolate (400 nm) plotted against reaction time (s). In all experiments, the reaction proceeds through three stages, indicated by three regions shown in the curve: induction region, redox reaction region, and wrap-up region. The induction time (t_0) was obtained by the coordinates of the point intersection of two tangential lines, which is dependent on the thiolate ligands adsorbed onto the gold nanoparticle surface. The net formation rate of 4-AP is zero in the induction region, during which spontaneous dynamic surface restructuring occurs, at the same time, the reducing reagent borohydride ions react with the surface of nanoparticles to form a surface-hydrogen species, pumping electrons to the metallic catalyst and lifting the Fermi energy level of the nanocatalyst.[34, 35] Raising the Fermi energy level alters oxidation potential of nanocatalyst and makes it capable of relaying electrons to 4-nitrophenolates to initiate the 4-NP/$NaBH_4$ redox reaction.[36, 37] The redox reaction region II starts when the peak at 300 nm is observed, which is accredited to the formation of 4-AP. Concomitantly, the intensity of 4-nitrophenolate peak is decreased sharply in this region, then becomes stagnant in region III (wrap-up region). During the wrap-up region, the formation rate of 4-AP approaches zero till the 4-nitrophenolates are consumed up.

3.4 Mechanism of 4-NP/$NaBH_4$ redox reaction catalyzed by alkylthiolate-stabilized PGMA@PAH@AuNPs composites

The mechanism of the 4-NP/$NaBH_4$ reduction catalyzed by alkylthiolate-stabilized PGMA@PAH@AuNPs composites is

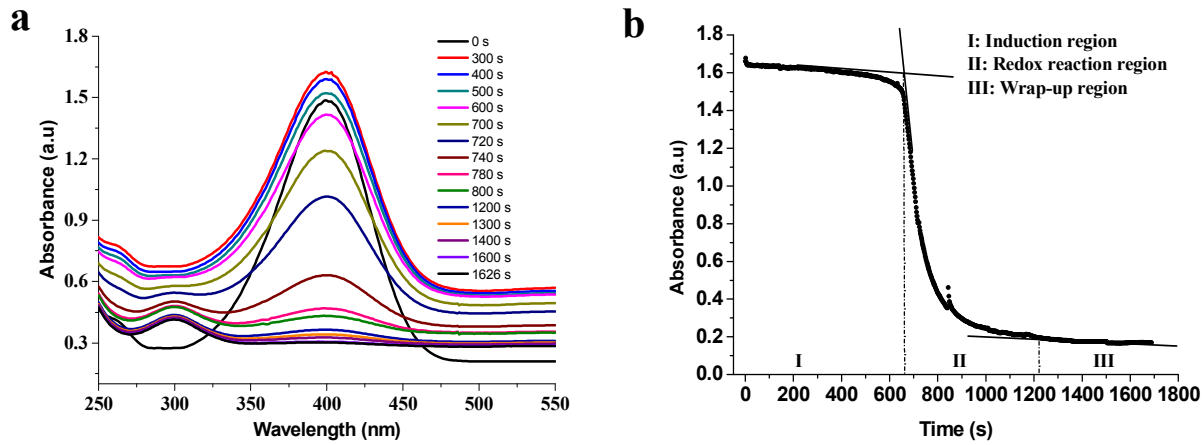

Figure 2 (a) Time–dependent UV-Vis spectra for the reduction of 4-NP in the presence of 6-mercaptohexanoic acid (0.113 mM) stabilized PGMA@PAH@AuNPs composites; (b) UV-Vis absorbance (400 nm) vs time plot for 4-NP/$NaBH_4$ reduction.

www.rsc.org/xxxxxx

ARTICLE TYPE

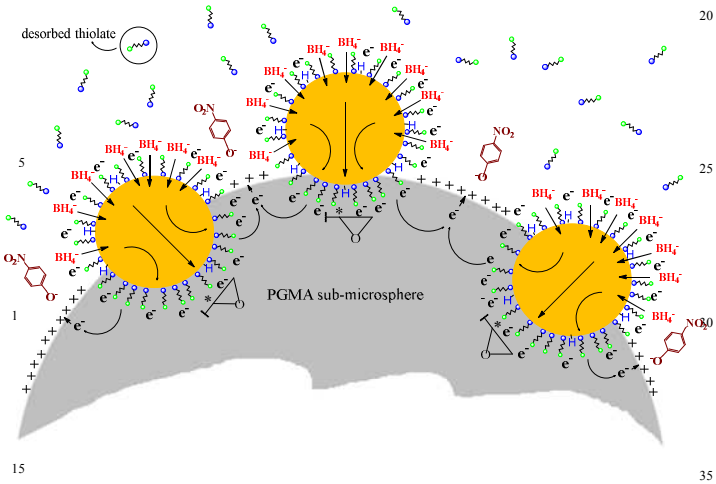

Schematic 2 Mechanism of 4-NP/$NaBH_4$ reduction in the presence of alkylthiolate-stabilized PGMA@PAH@AuNPs composite spheres.

illustrated in **Schematic 2** based on our previous publication,[2] which displays the essential process of the redox catalysis reaction as follows: borohydride ions react with gold nanoparticle surface forming surface-hydrogen species, during which electrons are injected onto gold nanoparticles. As noted, thiolate-stabilized gold nanoparticles exhibit a charge-depleted surface,[37-39] therefore, the more thiolate coverage is on gold nanoparticles surface, the higher tendency gold nanoparticles become attracted to electrons from the borohydride ions. Furthermore, epoxy groups of the PGMA spheres are prone to attract electrons and act as electron acceptors. Thus charge distribution occurs between the gold nanoparticles and PAH-modified PGMA spheres. Therefore, electrons leave the gold nanoparticles and end up with an electron-enriched region at the interface of gold nanoparticles and PAH-modified PGMA spheres. Meanwhile, the 4-nitrophenolate anion reactants can be easily adsorbed onto the positively charged PAH-modified PGMA spheres due to electrostatic interactions. The existence of the surplus electrons accumulated at the PGMA spheres facilitates

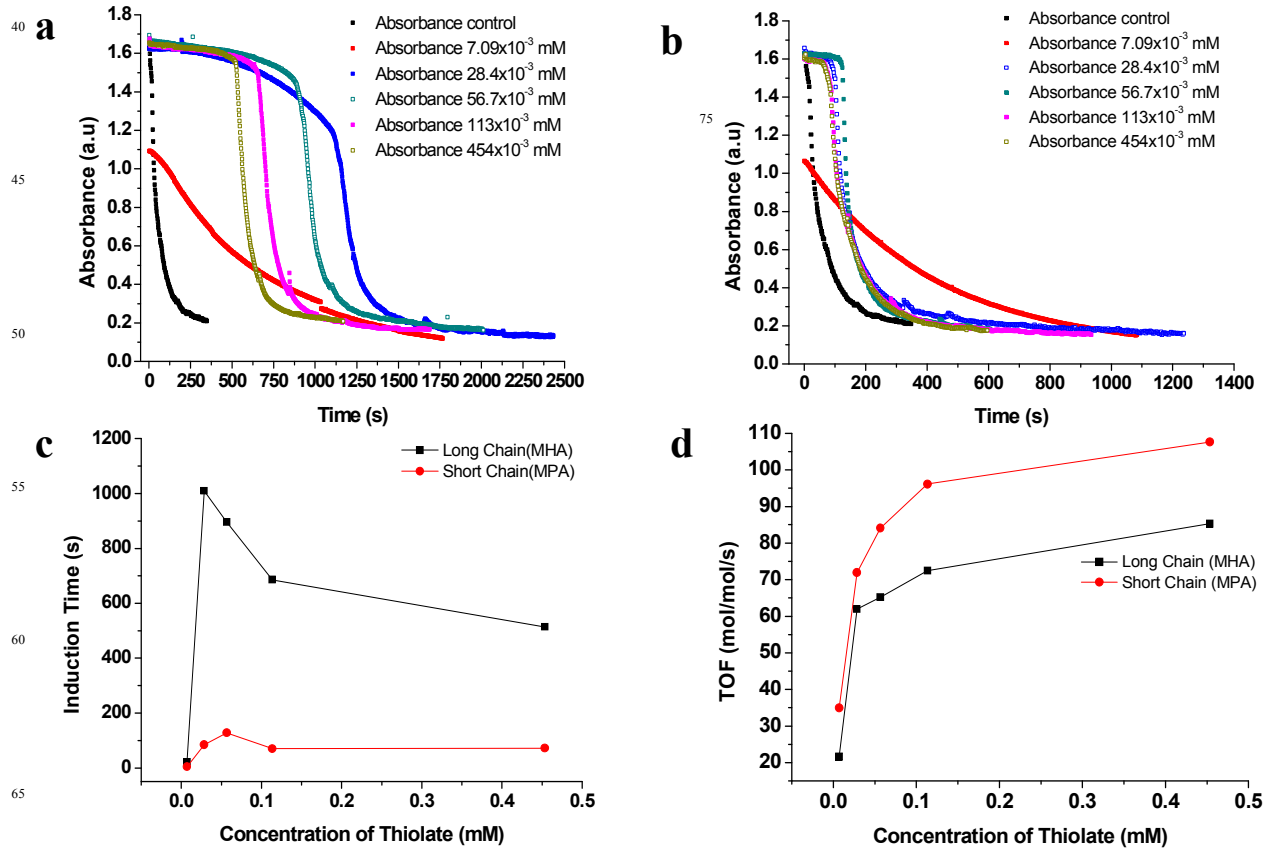

Figure 3 UV-Vis absorbance vs time plot for 4-NP/NaBH4 reduction in the presence of (a) 6-mercaptohexanoic acid (MHA) and (b) 3-mercaptopropionic acid (MPA) stabilized PGMA@PAH@AuNPs composites at various alkylthiolate concentrations; (c) Plot of induction time vs alkylthiolate concentration for MHA and MPA modified composite particles; (d) Turnover frequency (TOF) vs alkylthiolate concentration for MHA- and MPA-modified composite particles.

Table 1 Effects of long (MHA) and short (MPA) alkylthiolate modified composite particles on catalytic activity in 4-NP/$NaBH_4$ reaction

Thiolate concentration ($\times 10^{-3}$ mM)	t_0 (s)		Reaction Time (s)		R_{ave}[a] ($\times 10^{-10}$ mol·s^{-1})		TOF_{ave}[b] (mol·mol^{-1}·s^{-1})	
	MHA	MPA	MHA	MPA	MHA	MPA	MHA	MPA
Control	8	8	210	210	5.95	5.95	179.5	179.5
7.09	22	4	1,744	1,078	0.717	1.16	21.6	35.0
28.4	1,010	84	608	554	2.06	2.39	62.0	68.0
56.7	896	128	578	478	2.16	2.62	65.2	78.8
113	630	70	520	422	2.40	2.96	72.5	89.3
454	514	72	442	380	2.83	3.29	85.3	99.2

[a] denotes average reaction rate; [b] denotes average turnover frequency (TOF).

the uptake of electrons by the adsorbed 4-nitrophenol molecules, which leads to the reduction of 4-nitrophenol into the 4-aminophenol products. What's more, the strong reductant, sodium borohydride, desorbs alkylthiolate ligands from gold nanoparticle surface generating more active sites.[40] And detachment of the product 4-aminophenol creates a free surface as well, then the catalytic cycle can start again.

3.5 Effect of the graft density of surface alkylthiolate ligands

Induction time

The induction time, t_0, well exists in 4-NP/$NaBH_4$ redox reaction system catalyzed by the metal nanoparticle catalyst. In order to investigate the ligand thiolate effect on induction time and catalytic activity of PGMA@PAH@AuNPs composite particles, the water-soluble 6-mercaptohexianoic acid (MHA) or 3-mercaptopropionic acid (MPA) with –COOH as terminal groups was used to modify the composite particles. Thiolates are strong passivating agents due to strong covalent bonding to gold atoms. There exists a power correlation with a 2/3 scaling about the number of ligands molecules per gold atoms in thiolated gold nanoparticles.[41] Therefore, under the experiments performed here, the graft density of thiolate ligands on the gold nanoparticles surfaces is increased with the concentration of added alkylthiolate modifiers on the condition of unsaturated gold atoms. **Figure 3a, b** show the UV-Vis absorption spectra of MHA- and MPA-stabilized PGMA@PAH@AuNPs composite particles for 4-NP/$NaBH_4$ reduction reaction at absorbance of 400 nm against reaction time at various alkylthiolate surface coverage, respectively. As is seen in the spectra, there is always a time lag before any visible change in the absorbance value is observed. As the thiolate concentration for composite particles stabilized by MHA is 4 times increased from 7.09×10^{-3} to 2.84×10^{-2} mM, the induction time is increased from 22 to 1,010 s. When the thiolate stabilizer concentration for composite particles is further increased to 0.454 mM by 16 times, however, there is a twice decrease in induction time from 1,010 to 514 s. In the case of composite particles modified by MPA, similar trend is found when composites with thiolate concentration is increased from 7.09×10^{-3} to 5.67×10^{-2} mM, the induction time increases from 4 to 128 s, then decreases to 72 s with increasing thiolate concentration to 0.454 mM (**Table 1**). It can be explained based on spontaneous dynamic surface restructuring of the thiolate-modified gold nanoparticles[3, 14] and the $NaBH_4$ reducing agent requiring time for electron injection to gold nanoparticles surface.[11] When the composite particles have the lowest thiolate surface coverage, only a small portion of gold nanoparticle surface is occupied by the thiolate ligands and more bare gold atoms are exposed. Thus the spontaneous dynamic surface restructuring is relatively fast, and the electrons are not sterically hindered to be injected to gold nanoparticles surface from the reducing agent $NaBH_4$. Therefore, the induction time with very low thiolate ligand surface coverage becomes short, which shows almost no big difference from the control experiment (t_0 = 8 s for composites without alkylthiolate stabilizer involved). When thiolate surface coverage further increases, the induction time first increases tremendously, then decreases (**Figure 3c**). This observation is in agreement with SAM configuration above-mentioned: a relatively lower thiolate surface coverage favors a less-ordered "lying-down" SAM structure, which blocks access to most of actives sites and reduces the mobility of adsorbed thiolate ligands. As a result, the spontaneous dynamic surface restructuring of gold nanoparticles surface and the electron injection slow down. However, when thiolate surface coverage is further increased, a well-ordered "standing-up" SAM configuration will leave more active sites exposed with relatively less steric hindrance**,** therefore the spontaneous dynamic surface restructuring becomes faster, and reducing agents pump electrons to gold nanoparticle surface more efficiently, thus a truncated induction time is obtained.

Reaction time, average reaction rate and turnover frequency (TOF)

The activity of the alkylthiolate-stabilized composite catalysts decreases relatively to the original (no alkylthiolate coating) composite spheres. And the correlation between alkylthiolate surface coverage and catalytic activity is striking: a higher thiolate surface coverage leads to a shorter reaction time, higher average reaction rate and larger TOF for both MHA and MPA thiolate-stabilized cases (**Table 1**). Specifically, the 4-NP/$NaBH_4$ reduction reaction time is 210 s for the control experiment, but the reduction finishes in 1,744 s when MHA concentration is 7.09×10^{-3} mM, and runs faster as thiolate concentration further increases, and finally reaches 442 s when thiolate concentration goes up to 0.454 mM. Similar trend is seen from MPA-stabilized composites: reduction goes to completion in 1,078 s at the lowest thiolate concentration of 7.09×10^{-3} mM, and takes 380 s to wrap up at the highest thiolate concentration of 0.454 mM. Moreover, the average TOF of the control experiment is 179.5 mol·mol^{-1}·s^{-1}. However, as the thiolate concentration increases from 7.09×10^{-3} to 0.454 mM, the average TOF for MHA-stabilized composites increases from 21.6 to 85.3 mol·mol^{-1}·s^{-1}, while an increase from 35.0 to 99.2 mol·mol^{-1}·s^{-1} is observed for MPA-stabilized composites. **Figure 3d** manifests the trend of average TOF as a function of the concentration of alkylthiolate stabilizer coverage on gold nanoparticles catalysts. It indicates that the more alkylthiolate coverage on gold nanoparticles is there, the higher the TOF is, which correlates to the catalytic activity increasing with increased alkylthiolate surface coverage. This trend is also reflected from average reaction rate: the reduction becomes faster as the thiolate concentration increases for both MHA and MPA-stabilized composites. The average reaction rate increases

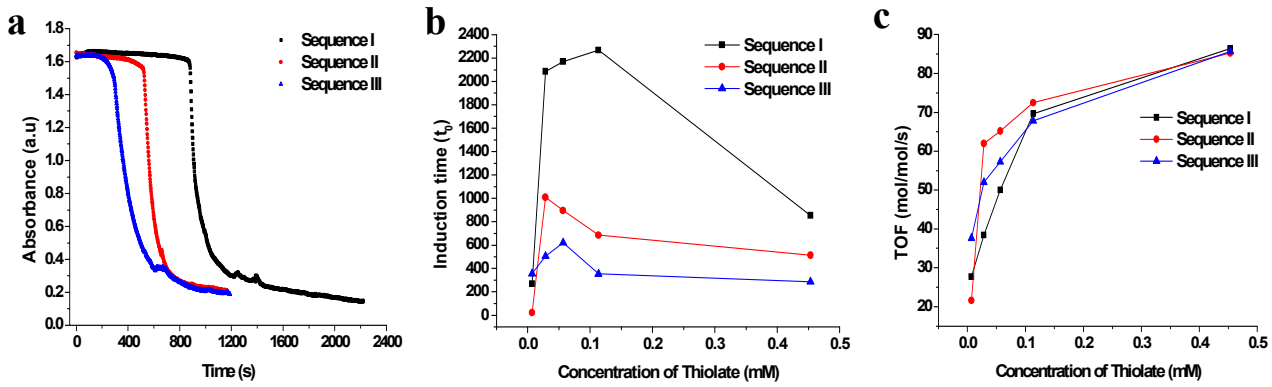

Figure 4 (a) Time-dependent UV-Vis absorbance (400 nm) vs time plot for 4-NP/$NaBH_4$ reduction in the presence of MHA (0.454 mM)-stabilized PGMA@PAH@AuNPs composites with different reactant addition sequences; (b) Plot of induction time vs. alkylthiolate concentration at different reactant addition sequences; (c) Plot of TOF vs. alkylthiolate concentration at different reactant addition sequences.

from 7.17×10^{-11} to 2.83×10^{-10} mol·s^{-1} for MHA-stabilized composites, and from 1.16×10^{-10} to 3.29×10^{-10} mol·s^{-1} for MPA-stabilized composites, when the thiolate concentration increases from 7.09×10^{-3} to 0.454 mM.

It is well-known that metal nanoparticle catalysts are easily poisoned by sulfur compounds.[42] When the thiolate is bound to gold nanoparticle surface forming stable surface metal sulphides, the active sites become inaccessible and the catalytic activity of the particles will be decreased. The increase in catalytic activity with increased alkylthiolate coverage can be explained by the sulfur-induced electronic charge-depleted state of gold surface.[43] Sulfur withdraws electrons from the metal and induces a decrease in its local charge density. For the alkylthiolate-stabilized PGMA@PAH@AuNPs composite spheres, there is a strong covalent interaction involving some sulfur-induced charge transfer from the gold nanoparticles to the thiolate functional groups. This leaves the gold atoms in the nanoparticles with depleted d charge at the gold sites. Gold nanoparticles with higher thiolate coverage will possess larger electron-deficient surfaces to activate the BH_4^- reductant more easily and facilitate the catalysis process, which will therefore result in shorter reaction time, larger magnitude of average reaction rate and TOF. It can be inferred that sulfur-gold interface also involves the catalytic activity.

3.6 Effect of chain length of surface alkylthiolate ligands

Although the graft density and chain order of alkylthiolate monolayers seem to control the induction phenomenon and the activity of the modified catalyst, the role of chain length of alkylthiolates should not be ignored, which is also a major determinant on the induction time and the catalyst activity (reaction time, average reaction rate and TOF).

Induction time

The initial induction stage related to t_0 involves two processes. First, the spontaneous dynamic surface restructuring of alkylthiolate-stabilized composite particles requires some time to become active for catalyzing redox reaction. Second, electron injection from reducing agent borohydrides to metal nanoparticles also contributes to the induction time. As can be seen in **Figure 3c**, when the thiolate surface coverage is at its lowest level, the induction time for longer alkylthiolate MHA is 22 s, which is over 5 times higher than that for shorter alkylthiolate MPA (4 s). At the concentration of 0.0567 mM of alkylthiolate, the induction time for MHA-stabilized composites is 896 s, around 7 times over that for MPA (128 s). The induction time for MHA-stabilized composites is 7 times higher than that for MPA when thiolate concentration is further increased to 0.454 mM (**Table 1**). It can be seen clearly that alkylthiolates with longer chain length have longer induction time throughout the whole range of the thiolate concentrations studied. This drastic difference could be ascribed to the following reasons: the increment of CH_2 in alkylthiolate chain results in a larger activation barrier deferring surface restructuring and steric hindrance effect elongating electron transfer time via surface hydrogen species from borohydride ions to gold nanoparticles. Thus the induction time is increased with increasing chain length of alkylthiolate stabilizers.

Reaction time, average reaction rate and TOF

The difference in reaction time for MHA and MPA stabilizers is not as large as that in induction time. However, the reaction time for MHA-stabilized composites is still 1.16~1.62 times longer than that for MPA throughout the thiolate concentration of 7.09×10^{-3} to 0.454 mM (**Table 1**). MPA-stabilized composites have a relatively higher average TOF than MHA at any constant thiolate surface coverage studied. The average TOF for MPA is 35.0 mol·mol^{-1}·s^{-1}, but 21.6 mol·mol^{-1}·s^{-1} for MHA-stabilized composites at the thiolate concentration of 7.09×10^{-3} mM. As the thiolate concentration is increased to 0.454 mM, the TOFs of 99.2 and 85.3 mol·mol^{-1}·s^{-1} are obtained for MPA and MHA respectively. At the low concentration of alkylthiolates of 7.09×10^{-3} mM, the average reaction rate for MPA-stablized composites is 1.16×10^{-10} mol·s^{-1}, but 7.17×10^{-11} mol·s^{-1} for MHA. As the thiolate concentration is increased to 0.454 mM, the average reaction rates of 3.29×10^{-10} and 2.83×10^{-10} mol·s^{-1} are obtained for MPA and MHA, respectively. The average rate of reaction and TOF increase with reduction in thiolate chain length (**Table 1**). A possible explanation is based on steric hindrance effect, namely, longer alkylthiolate chains induce more pronounced steric hindrance effect, which physically block access to active sites located at corners and edges of gold nanoparticle surfaces. Thus a shorter reaction time, higher reaction rate and greater TOF are achieved for short alkylthiolate ligand stabilizer.

3.7 Effect of reactant addition sequence

The addition sequence of 4-NP, $NaBH_4$ and the gold nanoparticles-based composite catalyst was also reported to affect the induction time and the catalytic activity of 4-NP/$NaBH_4$ redox reaction.[6]

www.rsc.org/xxxxxx

ARTICLE TYPE

Table 2 Effects of reactant addition sequence on catalytic activity in 4-NP/$NaBH_4$ reaction

MHA concentration ($\times 10^{-3}$ mM)	t_0 (s)			Reaction Time (s)			R_{ave} ($\times 10^{-10}$ mol·s^{-1})			TOF_{ave} (mol·mol^{-1}·s^{-1})		
	I[a]	II[b]	III[c]	I	II	III	I	II	III	I	II	III
7.09	270	22	357	1,360	1,744	1,002	0.919	0.717	1.25	27.7	21.6	37.6
28.4	2,086	1,010	506	981	608	725	1.27	2.06	1.72	38.4	62.0	52.0
56.7	2,170	896	620	753	578	658	1.66	2.16	1.90	50.0	65.2	57.3
113	2,268	685	354	541	520	556	2.31	2.40	2.25	69.7	72.5	67.8
454	894	514	286	436	442	440	2.87	2.83	2.84	86.4	85.3	85.7

[a] refers to Sequence I (4-NP+composites was mixed initially); [b] refers to Sequence II (4-NP+$NaBH_4$ was mixed initially); [c] refers to Sequence III ($NaBH_4$+composites was mixed initially). The details can be found in Experimental Section.

Herein, three different addition sequences namely, Sequence I, II and III (details can be found in Experimental Section) were designed to investigate their effect on the induction phenomenon and the catalytic activity. From **Figure 4** and **Table 2**, we can see that in all three addition sequences, the induction time increases first and then decreases with increasing the alkylthiolate stabilizer concentration. The average reaction rates and the TOFs become larger with the increase of the concentration of alkylthiolate stabilizer, which is consistent with the results obtained in the previous sections. At the lowest thiolate concentration of 7.09 × 10^{-3} mM, the induction time for Addition Sequence I and II are 270 and 22 s respectively, but 357 s for Addition Sequence III. When the thiolate concentration is increased to next level of 2.84 × 10^{-2} mM, the induction time for Addition Sequence I jumps up to 2,086 s, but only increases to 1,010 and 506 s for Addition Sequence II and III respectively. The reason for this 'weird' change is not clear, which needs further investigation. On the other hand, in a little higher concentration range of alkylthiolate stabilizer of 2.84 × 10^{-2} to 4.54 × 10^{-1} mM, the induction time is always larger for Addition Sequence I, but shorter for Addition Sequence II and III. In both Addition Sequence II and III, the reductant $NaBH_4$ is first added. This observation might be attributed to $NaBH_4$ reductant induced desorption of thiolate ligands.[44] The strong reduction ability of $NaBH_4$ can desorb the thiolate ligands from the gold nanoparticle surface leaving more surface area exposed, which offers quicker spontaneous dynamic surface restructuring of the composite catalysts and less steric hindrance for electron pumping from borohydride ions to the gold nanoparticles. Thus, the induction time is decreased a lot with the introduction of the strong reductant $NaBH_4$ to the reaction mixture firstly. At the same time, the data here also rule out the possibility of the effect of 4-NP-controlled diffusion on induction time, since in the Addition Sequence I, 4-NP has sufficient time to diffuse to the composite catalysts to decrease the induction time, but in fact, the longest induction time is found when 4-NP was mixed with composites initially. By further comparing the reaction time, the average reaction rates and the TOFs, there exist some differences at lower alkylthiolate stabilizer concentrations, but almost the same with higher stabilizer concentrations for all three Addition Sequences (**Table 2**). The reduction reaction goes to completion in ca. 440 s with an average reaction rate of ca. 2.8 × 10^{-10} mol·s^{-1} and the TOF of ca. 85.0 mol·mol^{-1}·s^{-1} when thiolate concentration is at the highest level of 0.454 mM for Addition Sequence I, II and III. The reasons behind this phenomenon are unclear, and further work need to be warranted.

4. Conclusions

Although much work has been done on the various aspects of alkylthiolate ligands to stabilize metal nanoparticles, little attention has been devoted to the study of the roles of alkylthiolate ligands for metal nanoparticles-coated polymer composite spheres as stabilizer and deactivator. The experimental and theoretical study presented in this paper, illustrated the effects of graft density, chain order and chain length on the induction time and the catalytic activity of the composite particles in heterogeneous reactions. Interestingly, we found the sulfur-gold interface also influenced the catalytic activity of the thiolate-stabilized metal nanoparticles. The results showed that the induction time appeared to be strongly correlated to the nature of aliphatic thiolate SAMs on gold nanoparticles surface and the addition sequence of reactants, namely, the increase in graft density of alkylthiolate ligand on metal nanocatalysts resulted in the increase first, and then decrease in induction time. And the shorter alkyl chain reduced induction time. Further, continuously enhanced catalytic activity was obtained with the increase of alkylthiolate graft density on composite particles, although the existence of alkylthiolate ligands deactivated the catalytic activity. And the longer alkyl chain length deteriorated their catalytic activity more greatly. Last, but not the least, study on reactant addition sequence revealed that the induction time was decreased a lot with the introduction of the strong reductant $NaBH_4$ to the reaction solution firstly, which can rule out the possibility of 4-NP diffusion-controlled induction time. This observation can be ascribed to borohydride reductant induced desorption of thiolate ligands. The kinetic and mechanistic

studies herein can guide the formation of SAMs on the alkylthiolate-stabilized PGMA@PAH@AuNPs composite particles to manufacture invaluable heterogeneous metal nanocatalysts.

Acknowledgements

We acknowledge St. John's University for the Seed Grant support. We are thankful to Xingru Yan and Prof. Zhanhu Guo from Lamar University for the TGA analysis. And we also thank Kim Kisslinger from Brookhaven National Laboratory for the help with TEM imaging. Research was carried out in part at the Center for Functional Nanomaterials, Brookhaven National Laboratory, which is supported by the U.S. Department of energy, Office of Basic Energy Sciences, under Contract No. DE-AC02-CH10886.

Reference

1 .M. M. Nigra, J.-M. Ha and A. Katz, *Catal. Sci. Technol.*, 2013, **3**, 2976-2983.
2. M. Li and G. Chen, *Nanoscale*, 2013, **5**, 11919-11927.
3. Wunder, F. Polzer, Y. Lu, Y. Mei and M. Ballauff, *J. Phys. Chem. C*, 2010, **114**, 8814-8820.
4. H. Yamamoto, H. Yano, H. Kouchi, Y. Obora, R. Arakawa and H. Kawasaki, *Nanoscale*, 2012, **4**, 4148-4154.
5. A. M. Signori, K. d. O. Santos, R. Eising, B. L. Albuquerque, F. C. Giacomelli and J. B. Domingos, *Langmuir*, 2010, **26**, 17772-17779.
6. A. M. Kalekar, K. K. K. Sharma, A. Lehoux, F. Audonnet, H. Remita, A. Saha and G. K. Sharma, *Langmuir*, 2013, **29**, 11431-11439.
7. X. Zhou, W. Xu, G. Liu, D. Panda and P. Chen, *J. Am. Chem. Soc.*, 2009, **132**, 138-146.
8. K. Kuroda, T. Ishida and M. Haruta, *J. Mol. Catal. A: Chem.*, 2009, **298**, 7-11.
9. J. Zeng, Q. Zhang, J. Chen and Y. Xia, *Nano Lett.*, 2010, **10**, 30-35.
10. S. Panigrahi, S. Basu, S. Praharaj, S. Pande, S. Jana, A. Pal, S. K. Ghosh and T. Pal, *J. Phys. Chem. C*, 2007, **111**, 4596-4605.
11. W. Xu, J. S. Kong, Y.-T. E. Yeh and P. Chen, *Nat. Mater.*, 2008, **7**, 992-996.
12. S. Wunder, Y. Lu, M. Albrecht and M. Ballauff, *ACS Catal.*, 2011, **1**, 908-916.
13. E. Gross, J. H.-C. Liu, F. D. Toste and G. A. Somorjai, *Nat. Chem.*, 2012, **4**, 947-952.
14. S. Wunder, Y. Lu, M. Albrecht and M. Ballauff, *ACS Catal.*, 2011, **1**, 908-916.
15. S. Panigrahi, S. Basu, S. Praharaj, S. Pande, S. Jana, A. Pal, S. K. Ghosh and T. Pal, *J. Phys. Chem. C*, 2007, **111**, 4596-4605.
16. G. Sharma and M. Ballauff, *Macromol. Rapid Commun.*, 2004, **25**, 547-552.
17. G. Weng, M. A. Mahmoud and M. A. El-Sayed, *J. Phys. Chem. C*, 2012, **116**, 24171-24176.
18. L. Yin and J. Liebscher, *Chem. Rev.*, 2007, **107**, 133-173.
19. Y. Mikami, A. Dhakshinamoorthy, M. Alvaro and H. Garcia, *Catal. Sci. Technol.*, 2013, **3**, 58-69.
20. W.-T. Liu, *J. Biosci. Bioeng.*, 2006, **102**, 1-7.
21. X. Yu and S. Ye, *J. Power Sources*, 2007, **172**, 145-154.
22. C. Vericat, M. E. Vela, G. Benitez, P. Carro and R. C. Salvarezza, *Chem. Soc. Rev.*, 2010, **39**, 1805-1834.
23. S. T. Marshall, D. K. Schwartz and J. W. Medlin, *Langmuir*, 2011, **27**, 6731-6737.
24. R. M. Crooks, M. Zhao, L. Sun, V. Chechik and L. K. Yeung, *Acc. Chem. Res.*, 2001, **34**, 181-190.
25. M. Biswas, E. Dinda, M. H. Rashid and T. K. Mandal, *J. Colloid Interface Sci.*, 2012, **368**, 77-85.
26. J. A. Lopez-Sanchez, N. Dimitratos, C. Hammond, G. L. Brett, L. Kesavan, S. White, P. Miedziak, R. Tiruvalam, R. L. Jenkins, A. F. Carley, D. Knight, C. J. Kiely and G. J. Hutchings, *Nat. Chem.*, 2011, **3**, 551-556.
27. E. Pensa, E. Cortés, G. Corthey, P. Carro, C. Vericat, M. H. Fonticelli, G. Benítez, A. A. Rubert and R. C. Salvarezza, *Acc, Chem. Res.*, 2012, **45**, 1183-1192.
28. Y. Liu, M. Li and G. Chen, *J. Mater. Chem. A*, 2013, **1**, 930-937.
29. Z. Luo, C. Zou, S. Syed, L. Syarbaini and G. Chen, *Colloid. Polym. Sci.*, 2012, **290**, 141-150.
30. J. Kimling, M. Maier, B. Okenve, V. Kotaidis, H. Ballot and A. Plech, *J. Phys. Chem. B*, 2006, **110**, 15700-15707.
31. J. Zhou, J. Ralston, R. Sedev and D. A. Beattie, *J. Colloid Interface Sci.*, 2009, **331**, 251-262.
32. E. Pensa, E. Cortes, G. Corthey, P. Carro, C. Vericat, M. H. Fonticelli, G. Benitez, A. A. Rubert and R. C. Salvarezza, *Acc. Chem. Res.*, 2012, **45**, 1183-1192.
33. H. Hakkinen, *Nat Chem*, 2012, **4**, 443-455.
34. M. A. Mahmoud and M. A. El-Sayed, *Nano Lett*, 2011, **11**, 946-953.
35. F. J. Vidal-Iglesias, R. M. Aran-Ais, J. Solla-Gullon, E. Herrero and J. M. Feliu, *ACS Catal.*, 2012, **2**, 901-910.
36. G. Weng, M. A. Mahmoud and M. A. El-Sayed, *J. Phys. Chem. C*, 2012, **116**, 24171-24176.
37. M. M. Nigra, J.-M. Ha and A. Katz, *Catal. Sci. Technol.*, 2013, **3**, 2976-2983.
38. J. Nara, S. i. Higai, Y. Morikawa and T. Ohno, *J. Chem. Phys.*, 2004, **120**, 6705-6711.
39. P. Zhang and T. K. Sham, *Phys Rev Lett*, 2003, **90**, 245502.
40. A. N. Zelikin, G. K. Such, A. Postma and F. Caruso, *Biomacromolecules*, 2007, **8**, 2950-2953.
41. A. Dass, *Nanoscale*, 2012, **4**, 2260-2263.
42. J. M. Jones, V. A. Dupont, R. Brydson, D. J. Fullerton, N. S. Nasri, A. B. Ross and A. V. K. Westwood, *Catalysis Today*, 2003, **81**, 589-601.
43. P. Zhang and T. K. Sham, *Phys. Rev. Lett.*, 2003, **90**, 245502/245501-245502/245504.
44. C. L. McCormick and A. B. Lowe, *Acc. Chem. Res.*, 2004, **37**, 312-325.